Hurricane Wave Topography and Directional Wave Spectra in Near Real-Time

Edward J. Walsh
NASA/Goddard Space Flight Center, Code 614.6
Wallops Flight Facility, Wallops Island, VA 23337
phone: (303) 497-6357 fax: (303) 497-6181 email: edward.walsh@nasa.gov

C. Wayne Wright
NASA/Goddard Space Flight Center, Code 614.6
Wallops Flight Facility, Wallops Island, VA 23337
phone: (443) 783-3319 fax: (757) 824-1036 email: charles.w.wright@nasa.gov

N0001406IP20037

LONG-TERM GOALS

Develop a simple parameterization for the directional wave spectrum in the vicinity of a hurricane.

OBJECTIVES

Develop and/or modify the real-time operating system and analysis techniques and programs of the NASA Scanning Radar Altimeter (SRA) to process the SRA wave topography data into directional wave spectra during hurricane flights. Upload the spectra and the topography onto a web site immediately post-flight to make them available to ONR investigators.

APPROACH

The SRA has a long heritage in measuring the energetic portion of the sea surface directional wave spectrum (Walsh et al. 1985; 1989; 1996, 2002; Wright et al. 2001). The wave spectra have recently been used to assess the output of a numerical wave model (Moon et al., 2003). To obtain the directional wave spectrum, the energy in the encounter spectrum generated from the SRA wave topography must be doubled everywhere, the artifact lobes deleted, and the real lobes Doppler-corrected. Identifying the artifact lobes for deletion and partitioning the real spectral lobes into the various wave components has been a slow and labor-intensive process. Edward J. Walsh has overall responsibility for developing the techniques and corrections to enable this analysis to be performed during the aircraft flights. C. Wayne Wright is responsible for the real-time operating system of the SRA and making whatever modifications are required to enable near real-time processing of the data.

WORK COMPLETED

SRA data acquisition concluded with the 2005 hurricane season. The effort since has focused on examining the general characteristics of hurricane wave fields, improving the SRA data processing, examining the effects of the finite footprint and backscattered power variations on the SRA wave spectra, assessing the performance of the WaveWatch III numerical wave model and looking for ways to combine the model and SRA observations to improve our knowledge of the sea surface conditions in the vicinity of hurricanes.

Report Documentation Page

Form Approved
OMB No. 0704-0188

1. REPORT DATE	2. REPORT TYPE	3. DATES COVERED
30 SEP 2006		**00-00-2006 to 00-00-2006**

4. TITLE AND SUBTITLE	5a. CONTRACT NUMBER
Hurricane Wave Topography and Directional Wave Spectra in Near Real-Time	5b. GRANT NUMBER
	5c. PROGRAM ELEMENT NUMBER
6. AUTHOR(S)	5d. PROJECT NUMBER
	5e. TASK NUMBER
	5f. WORK UNIT NUMBER
7. PERFORMING ORGANIZATION NAME(S) AND ADDRESS(ES) **NASA/Goddard Space Flight Center,Code 614.6,Wallops Flight Facility,Wallops Island,VA,23337**	8. PERFORMING ORGANIZATION REPORT NUMBER
9. SPONSORING/MONITORING AGENCY NAME(S) AND ADDRESS(ES)	10. SPONSOR/MONITOR'S ACRONYM(S)
	11. SPONSOR/MONITOR'S REPORT NUMBER(S)

12. DISTRIBUTION/AVAILABILITY STATEMENT
Approved for public release; distribution unlimited

13. SUPPLEMENTARY NOTES

14. ABSTRACT

15. SUBJECT TERMS

16. SECURITY CLASSIFICATION OF:			17. LIMITATION OF ABSTRACT	18. NUMBER OF PAGES	19a. NAME OF RESPONSIBLE PERSON
a. REPORT **unclassified**	b. ABSTRACT **unclassified**	c. THIS PAGE **unclassified**	**Same as Report (SAR)**	**12**	

RESULTS

Figure 1 indicates the dramatic azimuthal variation of hurricane directional wave spectra. In the center of the figure are wind speed contours (m/s) from the HRD HWIND surface wind analysis for a 2° box in latitude and longitude centered on the eye of Hurricane Ivan at 2230 UTC on 14 September 2004. The arrow at the center indicates Ivan's 330º direction of motion. The storm-relative locations of twelve directional wave spectra measured by the SRA are indicated by the black dots. Spectra have nine solid contours linearly spaced between 90% and 10% of peak spectral density, 5% contour is dashed. Dashed circles indicate wavelengths of 150, 250, and 350 m (outer to inner), solid circles are 200 and 300 m. Thick radials extend in the downwind direction a length equal to the wind speed at the 3 km aircraft altitude (m/s)*0.001. The upper number near the center of each spectrum is significant wave height, the lower number is distance from the center of the eye. The SRA data which produced the spectra were collected between 2030 UTC on 14 September 2004 and 0330 UTC on 15 September. The radial distance for the twelve spectral locations averaged 80 km. The unimodal wave field of 11.4 m height and 350 m wavelength in the right front quadrant (directly north of the eye) evolved into a bimodal and then trimodal wave system as the observation location rotated clockwise into the right rear quadrant (directly east of eye). The wave field transitioned back through bimodal to unimodal as the location rotated into the left rear quadrant, where the wave height and length were half the values in the right front quadrant. On the left side of the storm, the wind and wave directions are nearly orthogonal.

Recent SRA analysis has been focused on quantifying distortions of the wave spectra produced by variations in the power backscattered by the sea surface. The NOAA aircraft carrying the SRA was flown into hurricanes infrequently compared to the NOAA 6-hour forecast requirement. Even during CBLAST flights, SRA coverage was frequently limited by storm location. Ivan on 14 September 2004 had excellent azimuthal coverage (Fig. 1) because it was near Tampa. The NOAA aircraft had time to make six eye penetrations. In contrast, the first CBLAST SRA flight into Hurricane Frances made only two eye penetrations, providing one-third the azimuthal coverage. The WaveWatch III numerical wave model can provide hurricane wave fields at all locations and times, but it is critical to verify its performance. Combining measurements and wave model predictions can optimize benefits.

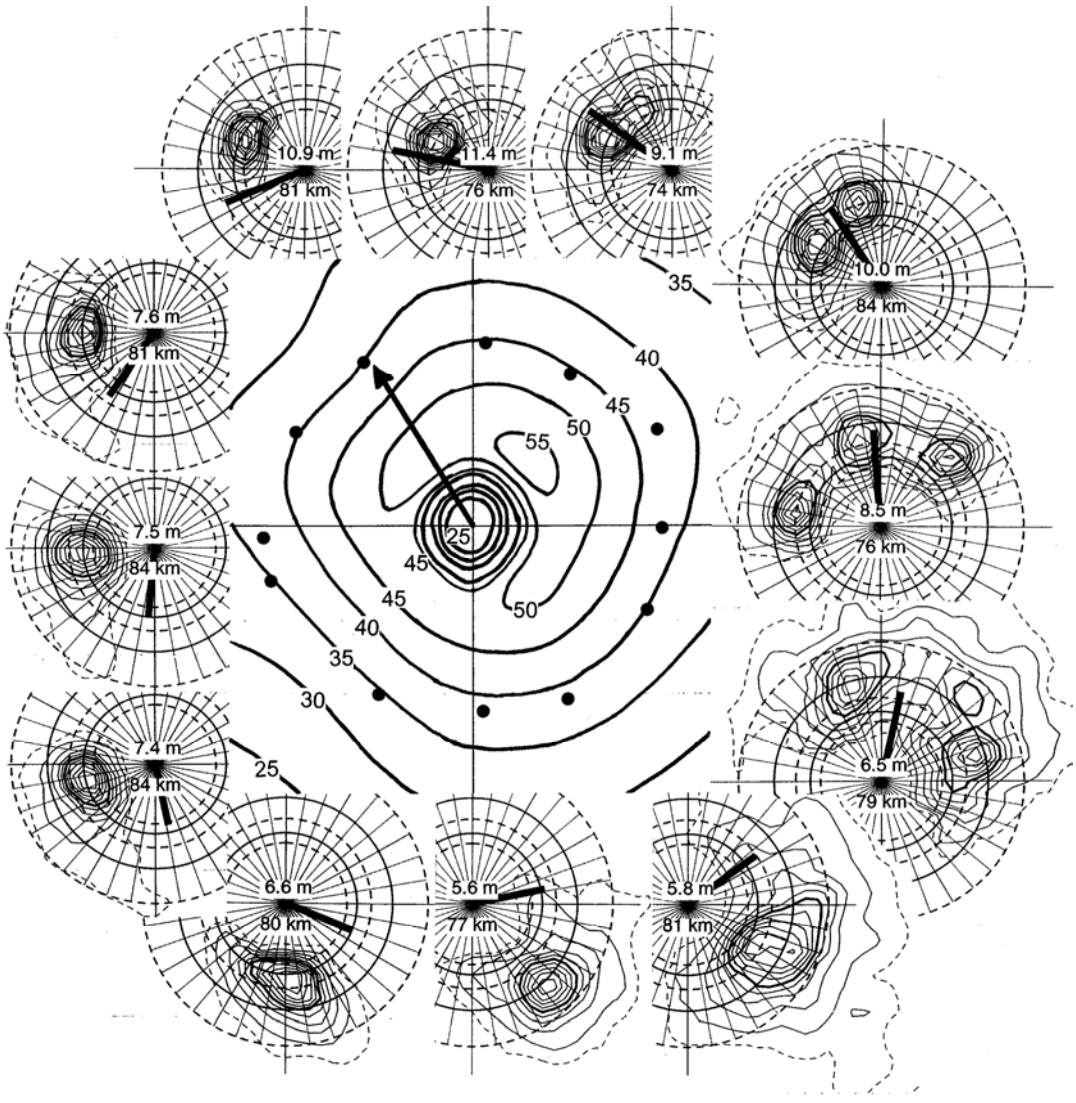

Figure 1. Azimuthal variation of the directional wave spectrum at about 80 km from the eye of Hurricane Ivan on 14 September 2004.

The SRA antenna scanned its 1° (two-way) antenna beam from 22° off-nadir to the left of the aircraft track, through nadir, to 22° off-nadir to the right, measuring the range to the sea surface at 64 cross-track positions at 15 Hz. The solid, parallel lines in Figure 2 show the 0.9 m half-power width bounds of the SRA pulse approaching the sea surface from 1500 m altitude. The horizontal sinusoidal curve represents an ocean wave of 50 m length and 1.67 m crest-to-trough height. The solid line orthogonal to the transmitted pulse indicates the antenna boresight and the dashed and dotted lines parallel to it indicate the half-power and 0.1 power limits of the 1° two-way antenna pattern, modeled as Gaussian.

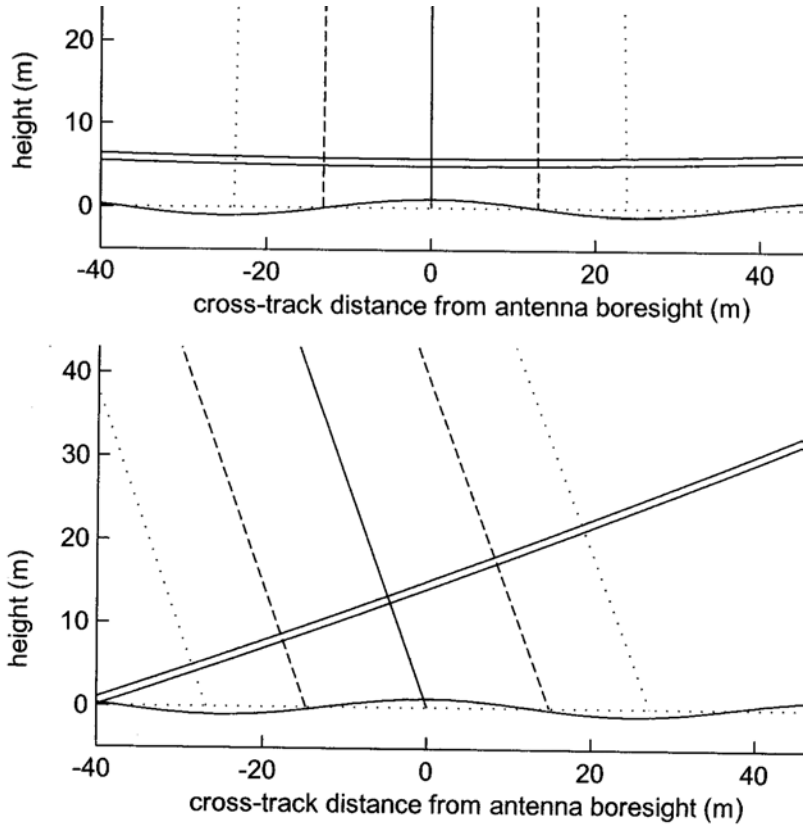

Figure 2. Nadir and off-nadir geometry for the SRA pulse transmitted from 1500 m height interacting with an ocean wave of 50 m length.

It is apparent that the centroid of the backscattered power for the pulse approaching the nadir point in the top panel will determine a range greater than that to the wave crest at the boresight because the half-power width of the antenna pattern extends to mean sea level. The reverse would be true for a trough at the boresight. This spatial filtering by the antenna footprint reduces the measured wave height at nadir.

In the bottom panel of Figure 2 the antenna boresight is 20° off-nadir. The wave crest at the boresight makes the local incidence angle 20° there, but places the maximum ±6° slopes of the 50 m length wave at the antenna half-power points. The local incidence angle is 26.5° at the off-nadir antenna half-power limit and 13.5° at the near-nadir limit. The smaller local incidence angle on the near-nadir side of the wave crest will increase the backscattered power and shift its centroid to shorter range. Ascribing the shorter range to the antenna boresight angle will increase the apparent height of the wave crest. If a wave trough were at the antenna boresight, the local incidence angle would be 15.5° at the off-nadir half-power antenna limit and 25.5° at the near-nadir limit. The lower local incidence angle on the off-nadir side of the trough would increase the backscattered power and shift the power centroid to longer range, indicating a deeper wave trough at the antenna boresight. Because the change in local incidence angle would be less for a trough at the boresight (10°) than for a crest (11°), the apparent trough deepening would be less than the apparent crest heightening, resulting in a slight rise in the sea surface.

Mean square slope (mss) is principally determined by the small scale sea surface roughness. The Plant (1982) theoretical maximum limit on mss at high wind speed is 0.080. It can become vanishingly small in the absence of wind and currents, but even in the eye of a hurricane there are still steep and breaking waves maintaining a lower limit of about 0.035. The top and middle panels of Figure 3 indicate how profiles of 50, 150, and 300 m waves propagating across the swath would be distorted for various off-nadir boresight angles and mss values of 0.080 and 0.035. All of the waves used in this SRA modeling effort were assumed to have a wavelength to crest-to-trough height ratio of 30:1. A wave of 300 m length would have a crest-to-trough height of 10 m. The solid curves in Figure 3 indicate the actual sinusoidal wave profiles normalized to unit amplitude. The various symbols indicate the apparent wave profiles that the SRA would determine from 1500 m altitude as a result of the variation of backscattered power with local incidence angle. For a 50 m ocean wavelength viewed at nadir, the measured profile would be reduced to about a quarter of its actual amplitude by the spatial filtering effect of the antenna footprint. As the incidence angle of the antenna boresight is increased, the enhancing effect of the variation of backscattered power with incidence angle increases and approximately compensates for the spatial filtering effect at 12° when the mss is 0.080 (top left panel of Figure 3). For larger incidence angles, the scattering distortion is greater than the spatial filtering effect and the apparent wave height is greater than the actual height. As the wavelength increases from 50 to 150 to 300 m, both distortions decrease because the sea surface varies less within the antenna footprint.

When mss is reduced to 0.035, the backscattered power changes more rapidly with incidence angle and that distortion increases, compensating for the spatial filtering effect when the antenna boresight is only 8° off-nadir (middle left panel of Figure 3). For a 16° off-nadir boresight, the wave crest appears to be 2.5 times its actual height whereas it appeared only 1.5 times its actual height when the mss was 0.080.

For waves propagating in the direction of the aircraft track, the SRA scans along the wave crest or trough and the sea surface slope is zero. The bottom panel of Figure 3 shows the results for that orientation and 0.035 mss. There is only spatial filtering by the footprint. For waves of 50 m length, the measure wave profiles are reduced at all incidence angles, but sea level appears to rise as the incidence angle is increased because of the variation of the backscattered power over the 1° beamwidth.

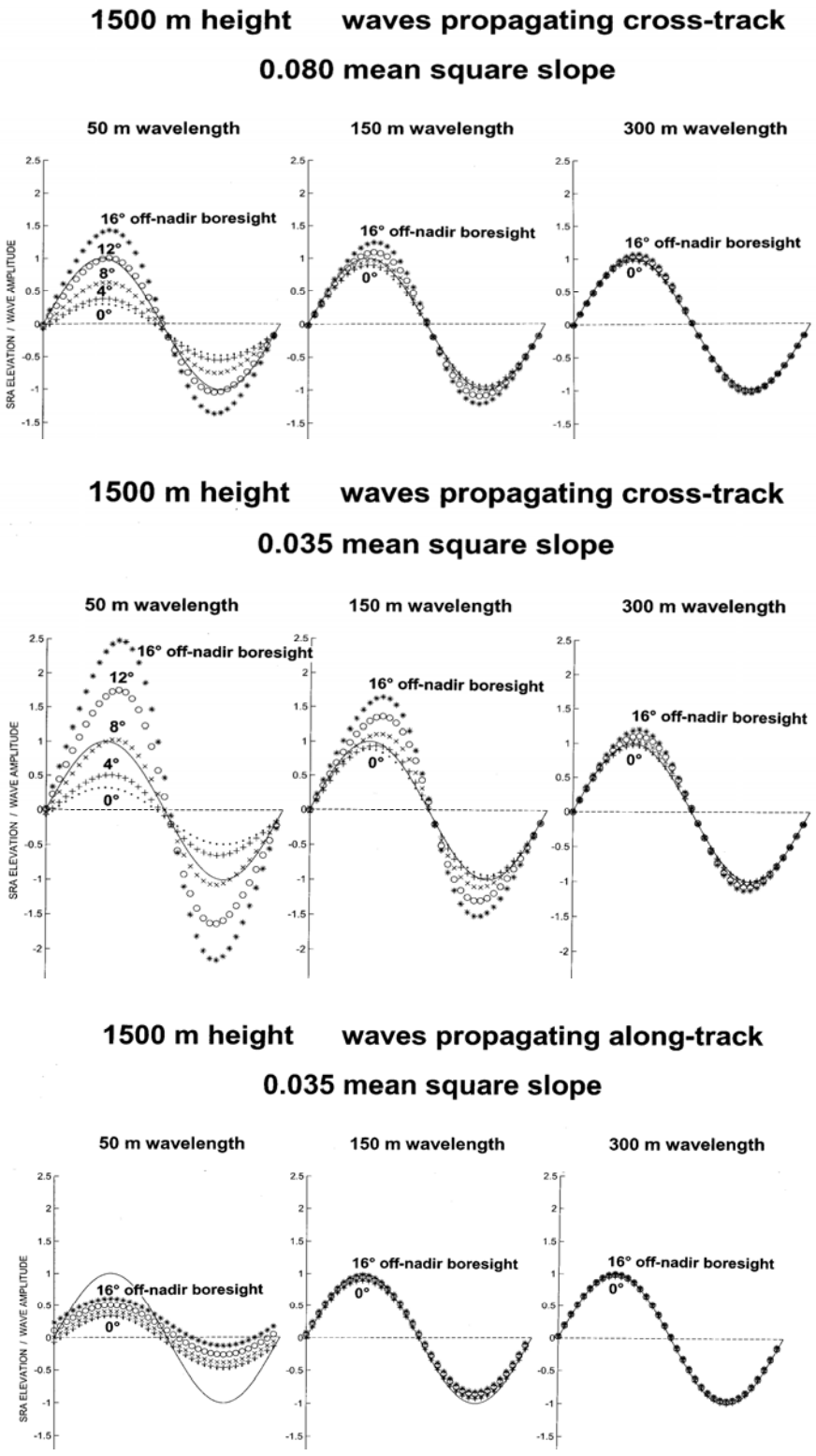

Figure 3. Modeled distortions of measured wave profiles for various values of surface roughness, incidence angle, ocean wavelength, and wave propagation direction.

The thick line in the top middle panel of Figure 4 shows the track of Hurricane Ivan on 9 September 2004 which was approximately toward 290°. The cluster of three circles on the Ivan track near 14.7°N, 71.8°W indicates the eye fixes made by the NOAA aircraft carrying the SRA. The thin line labeled A and B shows a portion of the NOAA aircraft track ahead of the storm. The aircraft was at 1500 m height initially flying perpendicular (A) to the Ivan track and subsequently turning parallel (B) to the track. The three circles on the aircraft track near A indicate the locations of the directional wave spectra on the left side of Figure 4. The three circles near B indicate the locations of the directional wave spectra on the right side of Figure 4. The nine solid contours vary linearly from the 90% to 10% in spectral energy density. The dashed contour is at the 5% level. The solid circles (outer to inner) on each spectra indicate ocean wavelengths of 100, 200 and 300 m. The dashed circles indicate wavelengths of 75, 150, 250 and 350 m. The long thick radial on each spectra indicates the wind speed at the aircraft 1500 m altitude divided by 1000. The dominant waves on the A leg averaged about 270 m in length and propagated toward about 290°. On the B legs the waves averaged about 320 m in length and propagated toward about 280°.

The short thick radial in each spectrum indicates the aircraft heading, which was approximately perpendicular to the wave propagation direction on leg A and parallel to it on leg B. Since the SRA antenna scan plane is perpendicular to the aircraft heading, the SRA was scanning approximately in the wave propagation direction on leg A (Figure 2, top and middle panels of Figure 3) and scanning approximately parallel to the wave crests and troughs on leg B (bottom panel of Figure 3). The middle center panel of Figure 4 shows the standard deviation of the SRA surface elevations along leg A as a function of cross-track position in the SRA swath. The standard deviations have been multiplied by 4 to convert them into significant wave height estimates. Ideally, there should be no variation with cross-track position for long data spans where the cross-track variation of the actual heights of the waves encountered would be statistically identical. On leg A the apparent wave height increased as soon as the antenna incidence angle deviated from nadir, as suggested by the top two panels of Figure 3

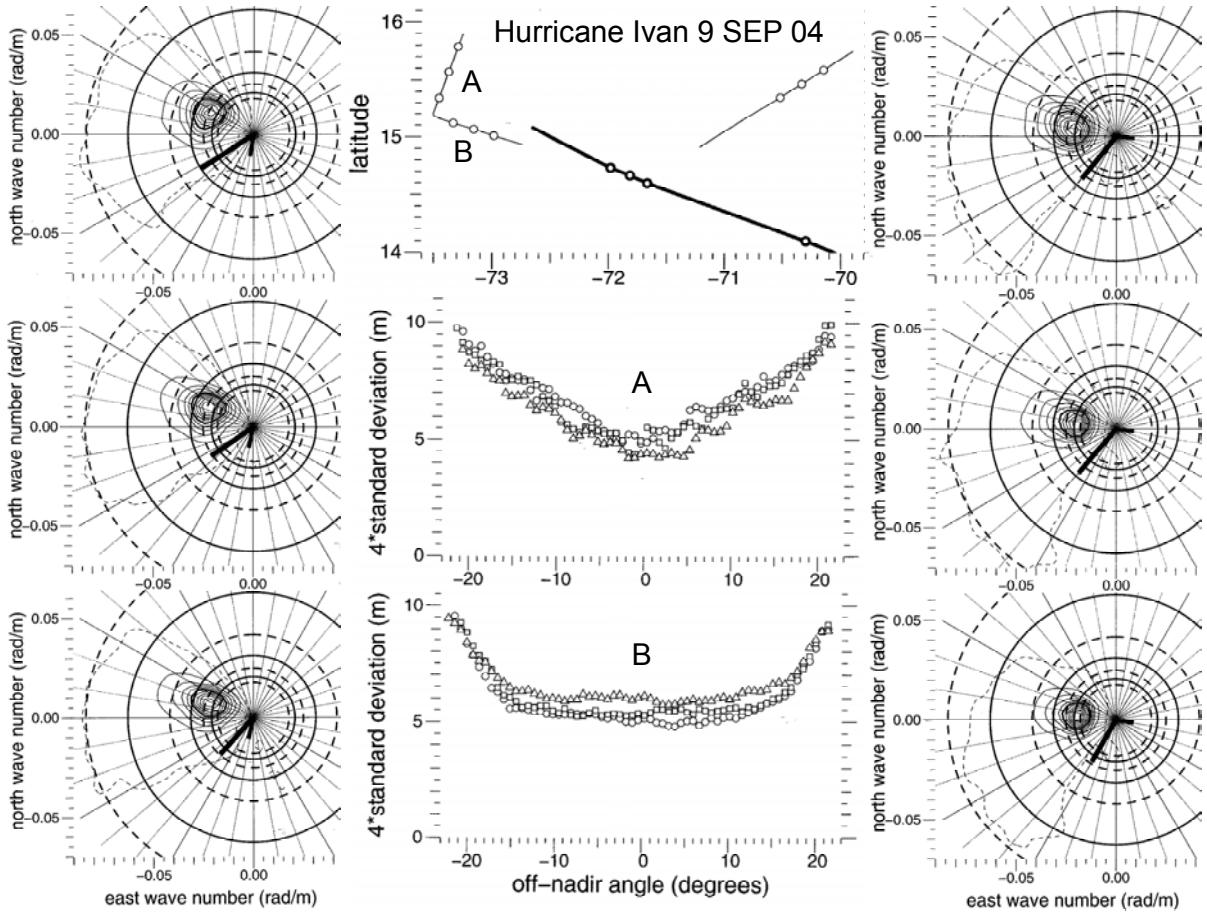

Figure 4. Directional wave spectra for waves propagating across the aircraft track (left panels, A) and along the aircraft track (right panels, B) and the variation of the measured sea surface height standard deviation across the SRA swath for the two orientations.

In contrast, the apparent wave height on leg B (bottom center panel of Figure 4) was nearly constant when the antenna boresight was within 15° of nadir, as suggested by the bottom panel of Figure 3. The reason the wave height increased for antenna boresights greater than 15° is due to the shorter wind-driven waves. Multiplying the wind speed at the aircraft altitude by 0.8 suggests that U_{10} on leg B was about 22 m/s. The dashed (5% of peak spectral density) contours in the B leg spectra shown on the right side of Figure 4 suggest there were wind-driven waves of 75 to 100 m length propagating across the SRA swath. Those waves were of lower height than the dominant waves and would also be subject to spatial filtering by the antenna footprint near nadir because of their shorter wavelength. But their tilt-modulation enhancement would greatly increase their apparent height for larger incidence angles and cause the apparent wave height to increase as the edge of the swath was approached.

While correction of the individual wave topography is not possible, corrections to spectral densities have been computed using the simulation that produced Figure 3. Those corrections have been applied to all the SRA wave spectra from the Ivan flight on 9 September 2004 and the results are compared with predictions of the WaveWatch III model (Isaac Ginis and Yalin Fan, GSO, University of Rhode Island, personal communication, 2006) in Figure 5. The top left panel of Figure 5 shows the NOAA

aircraft flight path through Ivan, whose track was toward 294°. Three eye penetrations were made. The first and third were at 2500 m height and the second was at 3000 m. Between eye penetrations the aircraft descended to 1500 m while repositioning. Just before departing the area, the aircraft descended to 1000 m height for a 100 km leg approximately parallel to the track of Ivan and displaced about 70 km to the right.

The top right panel of Figure 5 compares the propagation direction of the dominant waves predicted by WaveWatch III and observed by the SRA. To enable correlation with the aircraft position within Ivan, the aircraft track (degrees) is plotted in green and the aircraft height (m/10) is plotted in black. (The aircraft maintains a barometric altitude which resulted in about a 700 m decrease in actual height as the pressure minimum at the center of the eye was approached at spectrum numbers 43, 121 and 228). The agreement is excellent throughout the hurricane. Those places where the angles differ by more than 10° are generally in the left rear quadrant of the hurricane where, as indicated in Figure 1, there can be two or three comparable peaks in the observed spectrum with the maximum jumping back and forth among them. The WaveWatch III spectra were spaced at about 0.083° intervals in latitude and longitude and a two-dimensional interpolation was used on the wave model parameters to match the SRA spectral locations. The intermediate values of WaveWatch III propagation direction passing through 200° in the vicinity of spectra 115, 237 and 300 are artifacts resulting from that interpolation.

The lower left panel of Figure 5 compares the WaveWatch III model dominant wavelength and the SRA observations. Two systematic differences are apparent. First, behind the hurricane (spectra 1-40, 80-120, 230-300) the model dominant wavelength appears to be shorter than the SRA observations. Second, ahead of the hurricane (spectra 130-220) the model shows a slight oscillation in dominant wavelength that the SRA observations indicate is much larger. The minimum in the oscillation occurs near spectrum 170 in both model and measurements. The bottom right panel of Figure 5 compares the WaveWatch III model significant wave height and the SRA observations. The aircraft height (m/1000) is plotted in black and the aircraft track (degrees/100) is plotted in green. One systematic difference is apparent. On the right side of the hurricane (spectra 1-40, 150-220, 270-378) the model significant wave height appears to be higher than the SRA observations. Most of the apparent mismatch of wave height in spectra 40-120 could be eliminated by simply rotating the model azimuthal wave height minimum, which occurs in the left rear quadrant on approximately a 135° radial, about 27° clockwise.

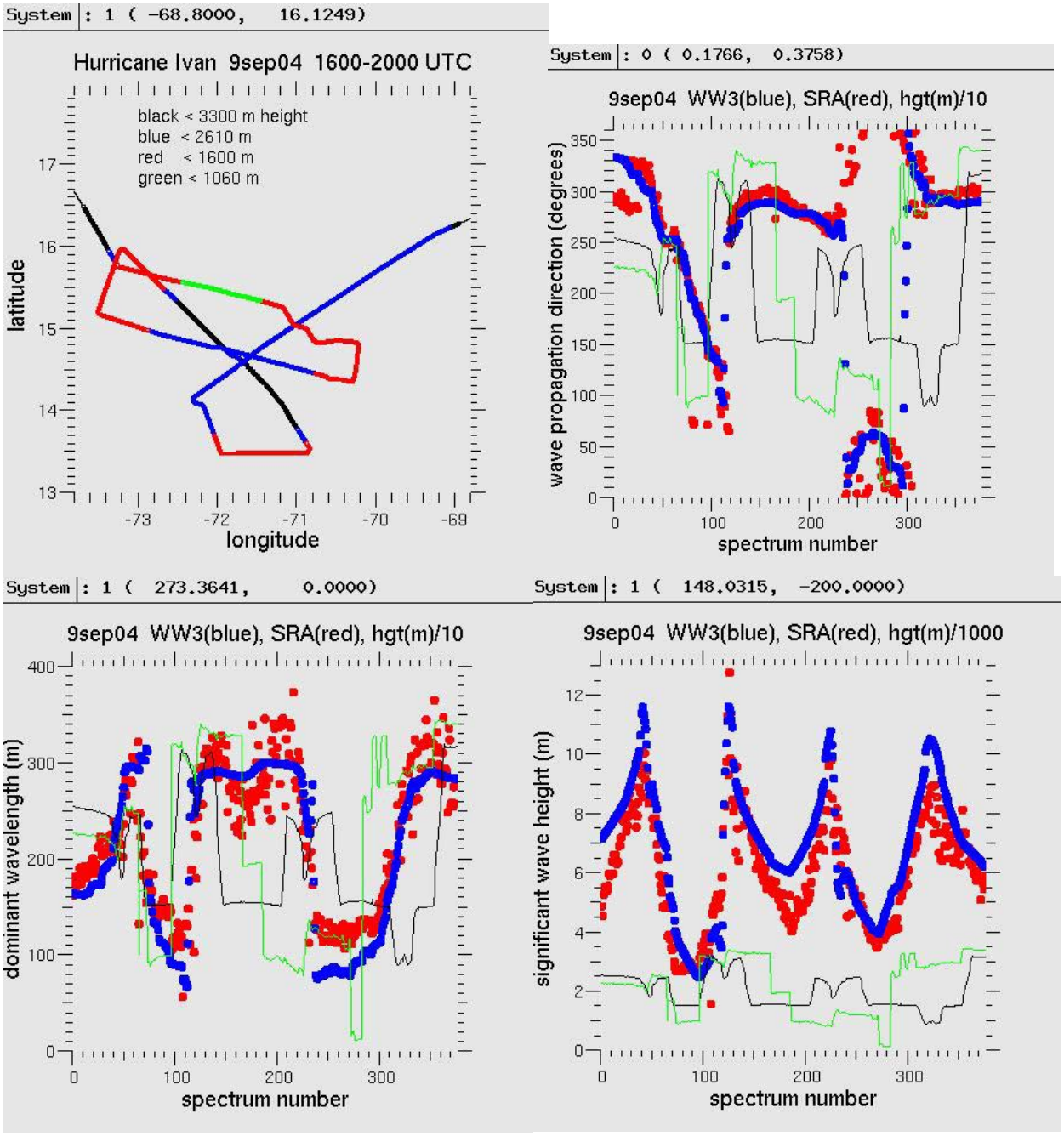

Figure 5. Aircraft flight track through Hurricane Ivan on 9 September 2004, color-coded for aircraft height (top left panel) and comparisons between SRA measurements and WaveWatch III predictions of significant wave height, dominant wavelength and wave propagation direction.

The circles in the left panel of Figure 6 indicate storm-relative locations of directional wave spectra from the SRA on the flight in Hurricane Ivan on 14 September 2004 when it was in the Gulf of Mexico. The six eye penetrations provided excellent azimuthal coverage (Figure 1) but the nominal aircraft altitude for the entire flight was 3000 m and much data was lost on the right side of Ivan due to rain attenuation. (The new NOAA SRA, which should be operational for the 2007 hurricane season,

will have higher signal level and operate at 16 GHz instead of the 36 GHz frequency used by the NASA SRA and be much less affected by rain.) The red line indicates the track of the ERS-2 and Envisat satellites which passed through Ivan about a half hour apart. The contours indicate the WaveWatch III wave height at 1-m intervals with the 17 m maximum contour located at 20 km east and 40 km north of the eye. The black line in the right panel of Figure 6 shows the WaveWatch III significant wave height along the satellite track. The red and blue dots indicate the values of wave height produced by the radar altimeters on the two satellites (Remko Scharroo, Altimetrics LLC, personal communication, 2006). The general agreement is good, although there are places where WaveWatch III tends to be high relative to the satellite altimeters and the SRA tends to be low.

The next step in the analysis is a detailed spectra by spectra comparison to sort out the discrepancies observed and determine reasons for them. The result will be an increased confidence in using the wave model to predict such things as the breaking probability throughout a hurricane (Banner et al., 2000).

IMPACT/APPLICATIONS

The SRA provided the first comprehensive, quantified measurements of the directional wave spectrum spatial variation in the vicinity of hurricanes. The data impact all assessments of air/sea interaction in a hurricane environment and serve to validate wave models. The ability to examine the structure of individual waves and wave groups is important for assessing viability of marine structures.

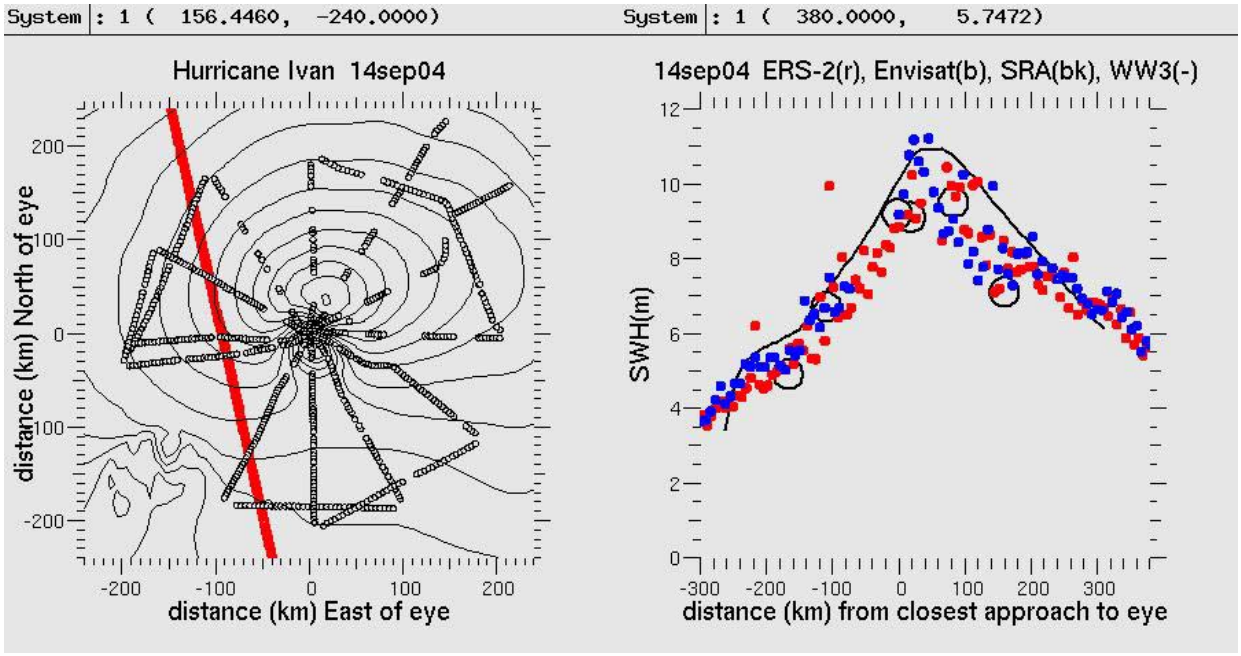

Figure 6. The circles in the left panel indicate storm-relative locations of SRA directional wave spectra and the red line indicates the track of Envisat and ERS-2 which was approximately parallel to the track of Ivan and displaced about 90 km to the left. The right panel shows values of wave height predicted by WaveWatch III and measured by the SRA and the satellite radar altimeters.

RELATED PROJECTS

All hurricane components of ONR CBLAST.

REFERENCES

Banner, M. J., A. V. Babanin, I. R. Young, 2000: Breaking probability for dominant waves on the sea surface, J. Phys. Oceanogr., 30, 3145-3160.

Moon, Il-Ju, Isaac Ginis, Tetsu Hara, Hendrik L. Tolman, C. W. Wright and Edward J. Walsh, 2003: Numerical simulation of sea surface directional wave spectra under hurricane wind forcing, J. Phys. Oceanogr., 33, 1680-1706.

Plant, W. J., 1982: A relationship between wind stress and wave slope, J. Geophys. Res., 87, 1961-1967.

Walsh, E. J., D. W. Hancock, D. E. Hines, R. N. Swift, and J. F. Scott, 1985: Directional wave spectra measured with the surface contour radar, J. Phys. Oceanogr., 15, 566-592.

Walsh, E. J., D. W. Hancock, D. E. Hines, R. N. Swift, and J. F. Scott, 1989: An observation of the directional wave spectrum evolution from shoreline to fully developed, J. Phys. Oceanogr., 19, 670-690.

Walsh, E. J., L. K. Shay, H. C. Graber, A. Guillaume, D. Vandemark, D. E. Hines, R. N. Swift, and J. F. Scott, 1996: Observations of surface wave-current interaction during SWADE, The Global Atmosphere and Ocean System, 5, 99-124.

Walsh, E. J., C. W. Wright, D. Vandemark, W. B. Krabill, A. W. Garcia, S. H. Houston, S. T. Murillo, M. D. Powell, P. G. Black, F. D. Marks, 2002: Hurricane directional wave spectrum spatial variation at landfall, J. Phys. Oceanogr., 32, 1667-1684.

Wright, C. W., E. J. Walsh, D. Vandemark, W. B. Krabill, A. Garcia, S. H. Houston, M. D. Powell, P. G. Black, and F. D. Marks, 2001: Hurricane directional wave spectrum spatial variation in the open ocean, J. Phys. Oceanogr., 31, 2472-2488.

PUBLICATIONS

Black, P. G., E. A. D'Asaro, W. M. Drennan, J. R. French, P. P. Niiler, T. B. Sanford, E. J. Terrill, E. J. Walsh and J. Zhang, 2006: Air-sea exchange in hurricanes: synthesis of observations from the Coupled Boundary Layer Air-Sea Transfer Experiment, Bull. Amer. Meteor. Soc., 87, [in press, refereed].

Chen, S. S., J. F. Price, W. Zhao, M. A. Donelan, E. J. Walsh, 2006: The CBLAST-Hurricane Program and the next-generation fully coupled atmosphere-wave-ocean models for hurricane research and prediction, Bull. Amer. Meteor. Soc., 87, [in press, refereed].